Supporting Information for

Self-Assembled Carbon Dot-Wrapped Perovskites Enable Light Trapping and Defect Passivation for Efficient and Stable Perovskite Solar Cells

Ngoc Duy Pham[1,2], Amandeep Singh [1,2], Weijian Chen[4], Minh Tam Hoang [1,2], Yang Yang [1,2], Xiaodong Wang[2,3], Annalena Wolff[3], Xiaoming Wen[4], Baohua Jia[4], Prashant Sonar [1,2], and Hongxia Wang [1,2 *]

[1] School of Chemistry and Physics, Science and Engineering Faculty, Queensland University of Technology, Brisbane, QLD 4001, Australia

[2] Centre for Materials Science, Queensland University of Technology, Brisbane, QLD 4001, Australia

[3] Central Analytical Research Facility, Institute for Future Environments, Queensland University of Technology, Brisbane, QLD, 4001 Australia

[4] Centre for Translational Atomaterials, Swinburne University of Technology, Melbourne, VIC 3122, Australia

Corresponding author:

*E-mail: hx.wang@qut.edu.au

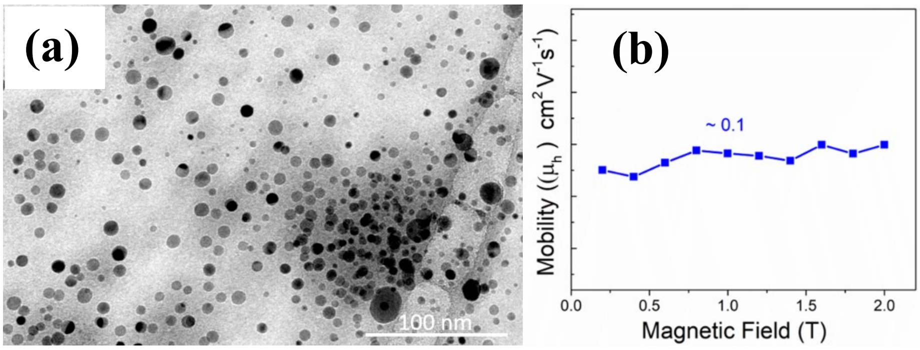

Figure S1. Size and hole mobility of carbon dots (CDs) derived from human hair. (**a**) TEM image. (**b**) hole mobilities of CDs film with varying magnetic field at room temperature.

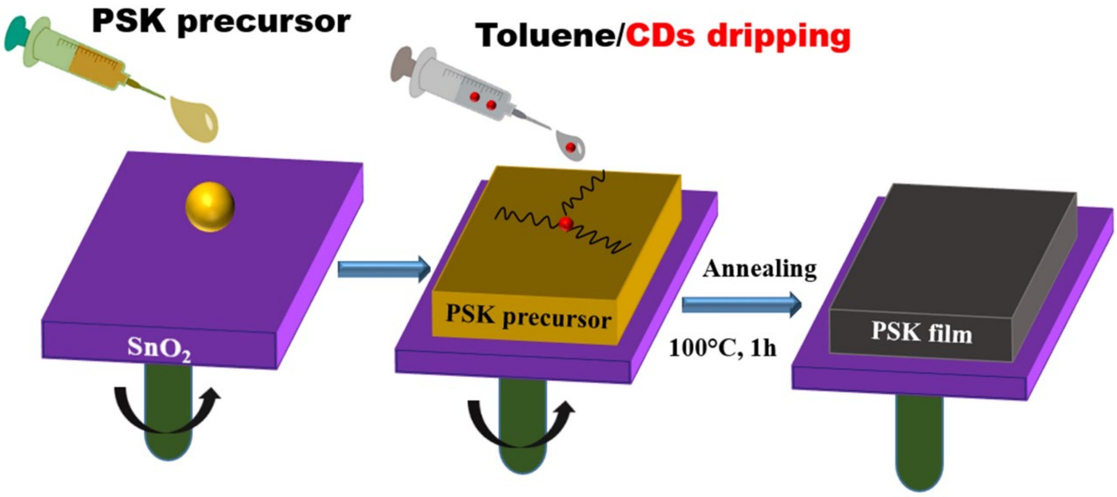

Figure S2. Schematic diagram of the anti-solvent dripping based synthesis of $Cs_{0.05}FA_{0.80}MA_{0.15}PbI_{2.55}Br_{0.45}$ perovskite films

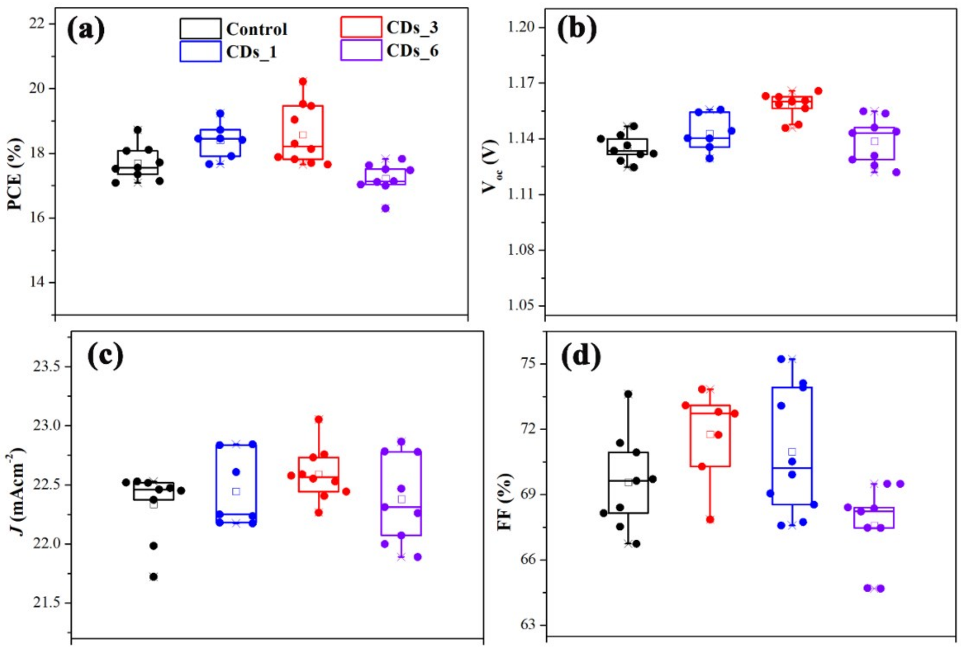

Figure S3. Statistical performance of PSCs made with various CDs contents (0 – 6 mg/mL): (**a**) power conversion efficiencies; (**b**) open-circuit voltages; (**c**) current densities; (**d**) fill-factors.

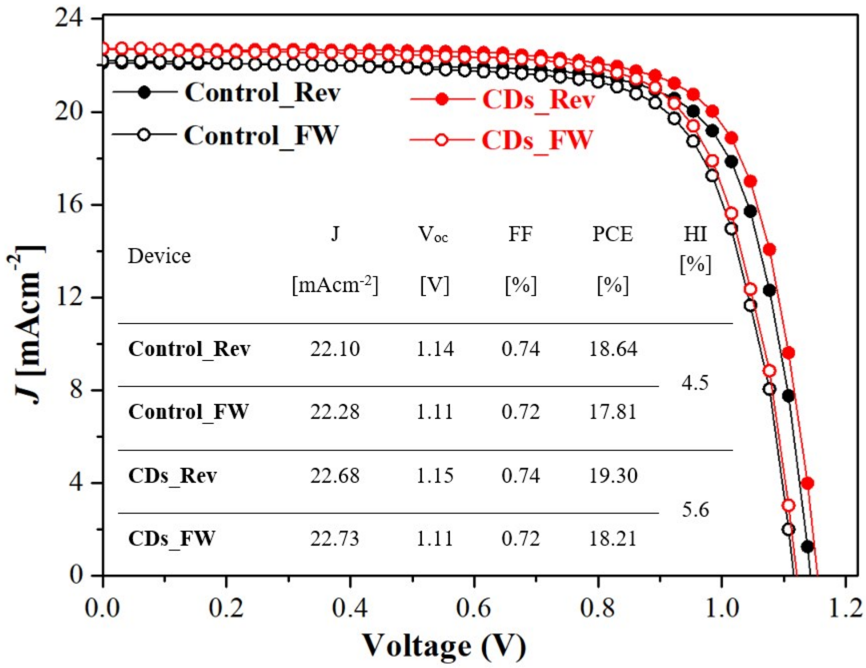

Device	J [mAcm^{-2}]	V_{oc} [V]	FF [%]	PCE [%]	HI [%]
Control_Rev	22.10	1.14	0.74	18.64	4.5
Control_FW	22.28	1.11	0.72	17.81	
CDs_Rev	22.68	1.15	0.74	19.30	5.6
CDs_FW	22.73	1.11	0.72	18.21	

Figure S4. Hysteresis behaviour of PSCs. Rev and FW scans represent the measurements following the voltage sweeps from open-circuit to short-circuit and from short-circuit to open-circuit condition, respectively.

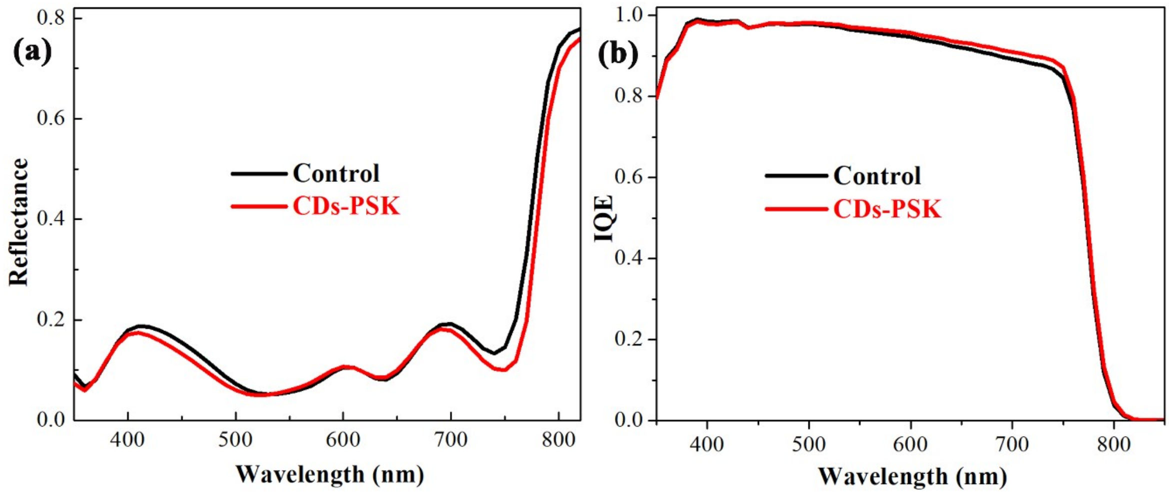

Figure S5. (**a**) Specular reflectance and (**b**) internal quantum efficiency (IQE) spectra of PSCs

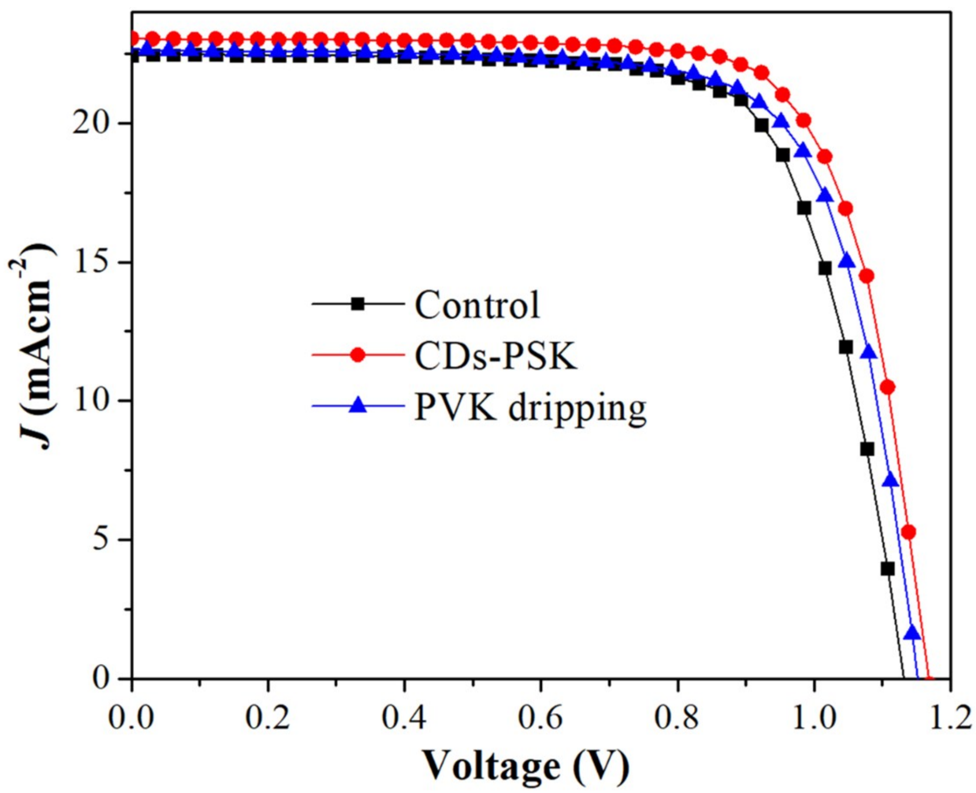

Figure S6. J-V characteristics of devices made using antisolvent based on: pure toluene (black curve), 1 mg/mL Poly(9-vinylcarbazole) in toluene (blue curve), 1 mg/mL Poly(9-vinylcarbazole) and 3 mg/mL CDs in toluene (red curve).

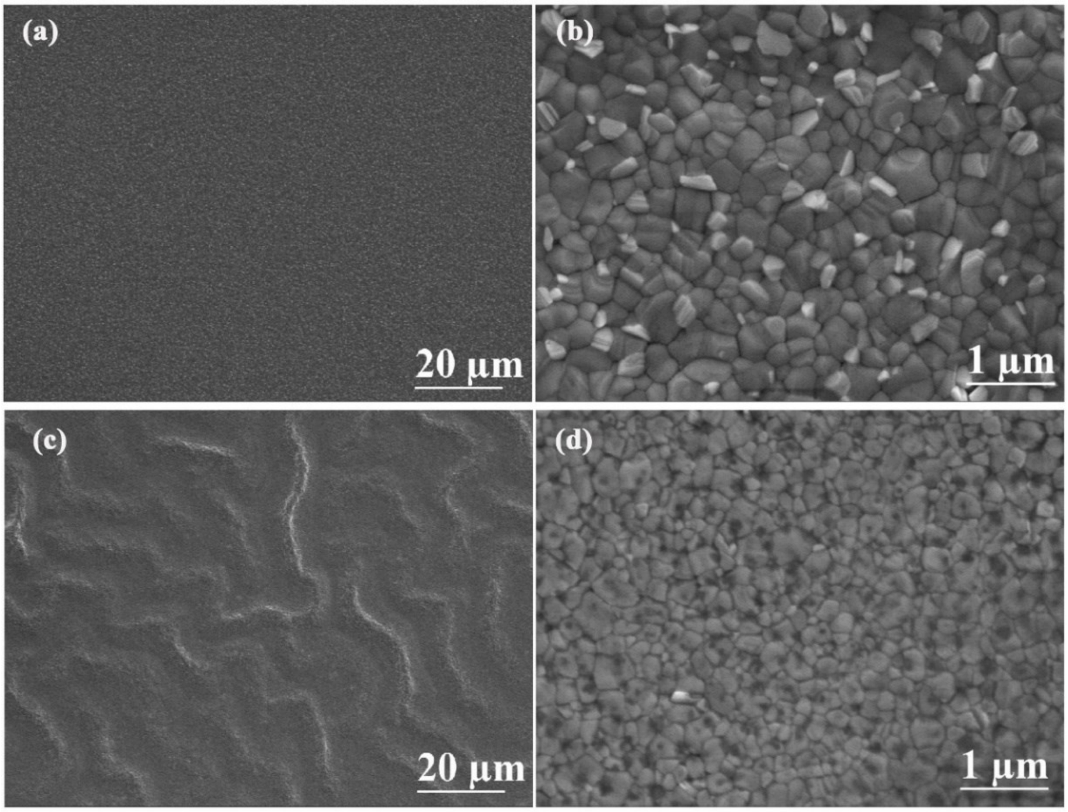

Figure S7. Top-view SEM images of control perovskite (**a** and **b**) and CDs-PSK film (**c** and **d**). A statistical evaluation of 200 grains for both images (**Figure S7-(b** and **d**)) shows that the average grain size for the CD-PSK film, 220nm ± 95 nm is considerably smaller than that for the control film, 299nm ±111 nm.

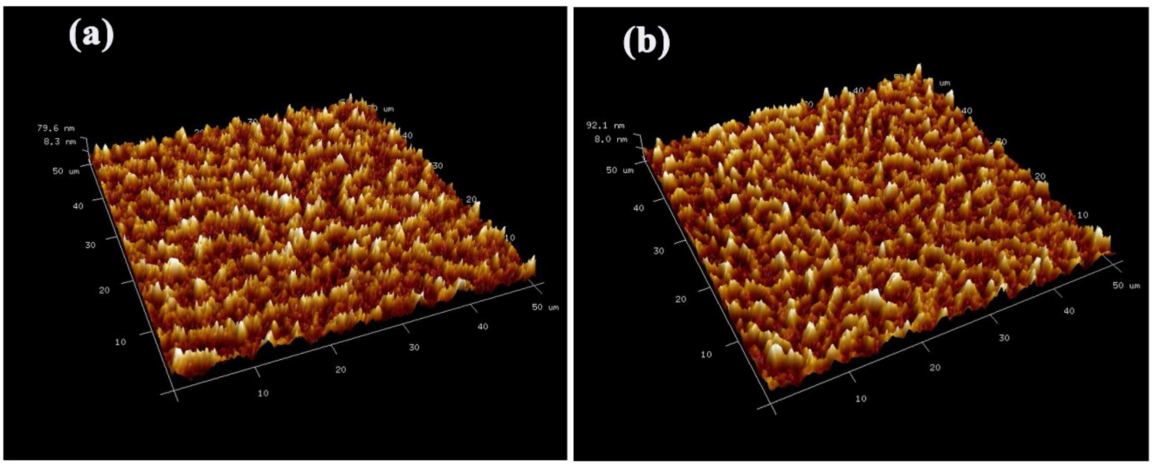

Figure S8. Three-dimensional atomic force microscopy images for perovskite film fabricated wit (**a**) 1 mg/mL and (**b**) 2 mg/mL Poly(9- vinylcarbazole) in toluene.

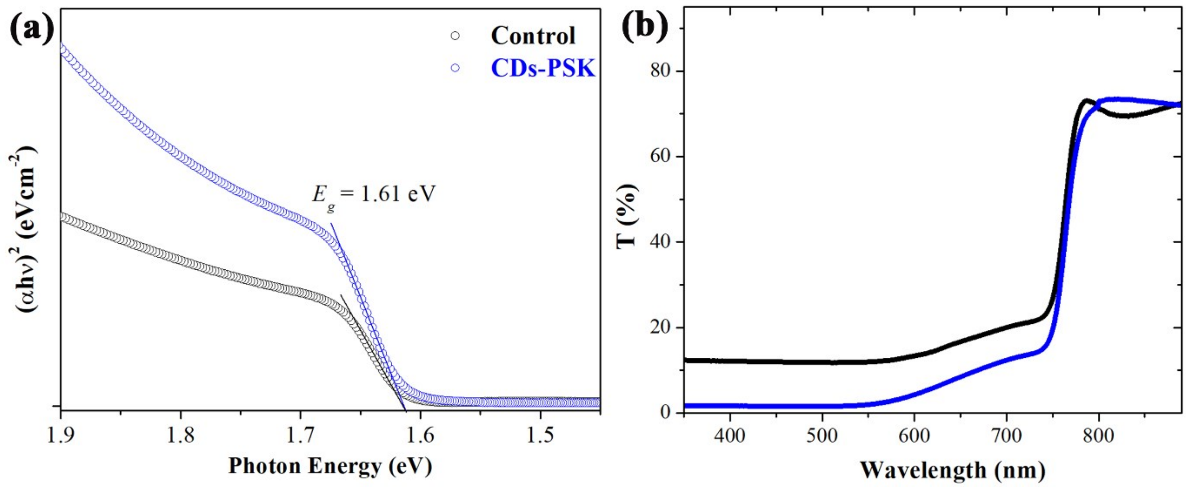

Figure S9. (**a**) Estimated bandgap, and (**b**) transmission spectra perovskite films

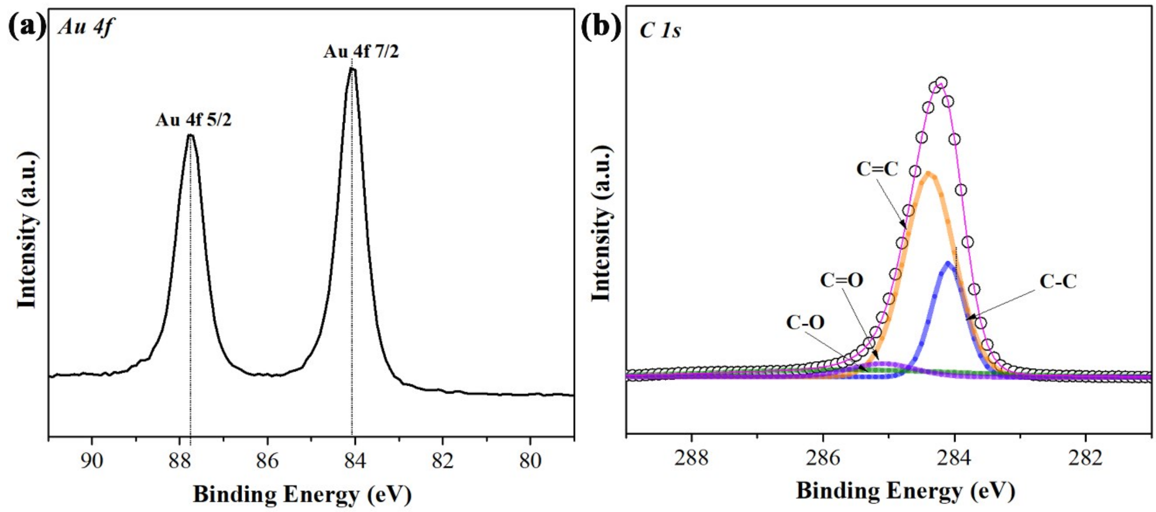

Figure S10. High resolution XPS of (**a**) the Au 4f core level for the Au reference film and (**b**) C 1s core level for the CDs film on deposited on FTO substrate.

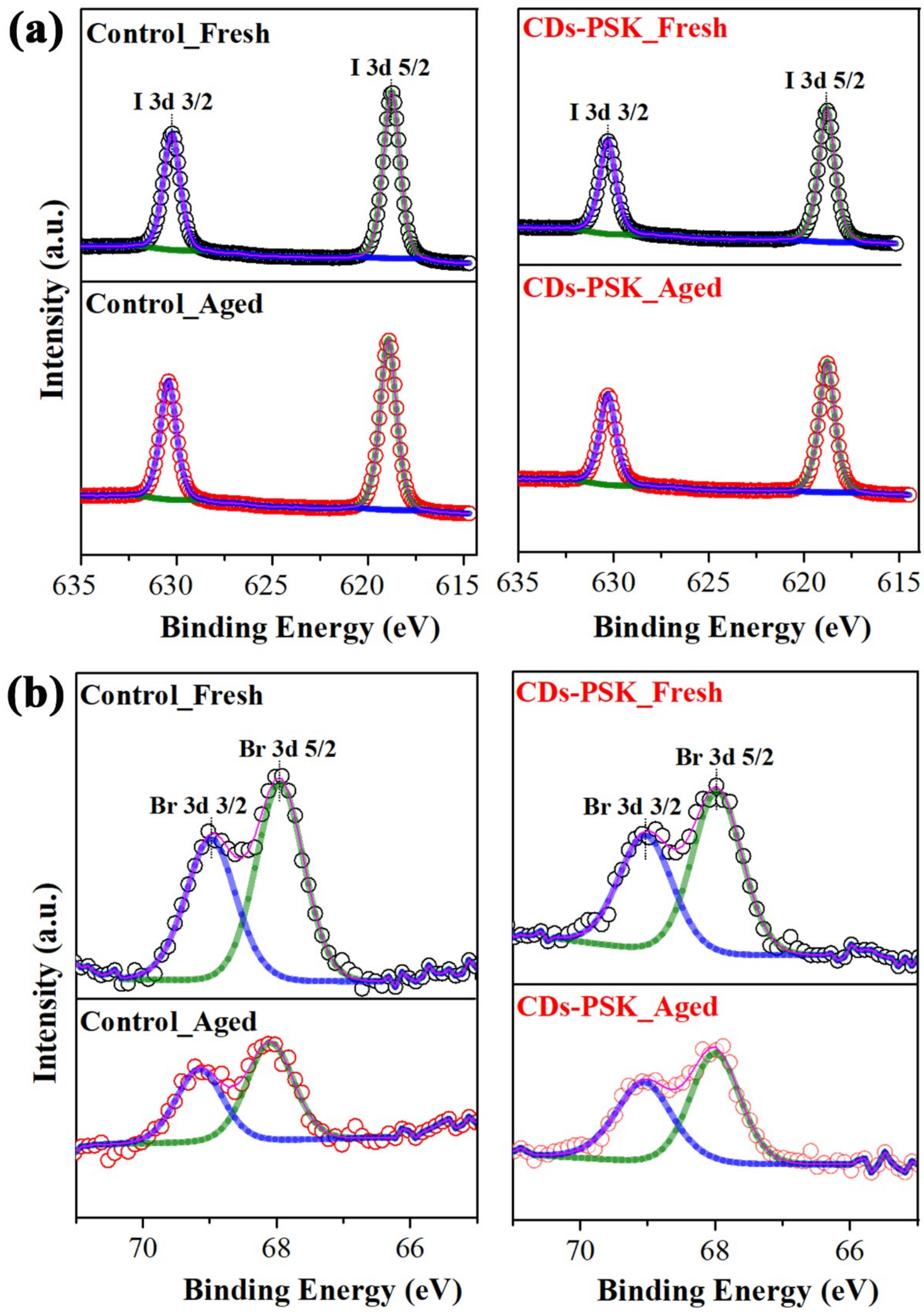

Figure S11. High resolution X-ray photoelectron spectroscopy spectra (Al−Kα = 1486.6 eV) and fittings of (**a**) I 3d and (**b**) Br 3d core levels for the perovskite films.

Table S1. Peak positions of high resolution XPS data.

Element	**Peak position (eV)**	**Attributed bonding environments**
Control (Fresh)		
C 1s	284.1/286.7/287.9	C-C/C-N/C=N
Pb 4f	137.9/142.8	Pb^{2+}
Pb 0	136.2/141.1	Pb^{0}
I 3d	618.7/630.2	I^{-}
Br 3d	68.0/69.0	Br^{-}
Control (Aged)		
C 1s	284.1/286.5/288	C-C/C-N/C=N
Pb 4f	138.1/142.9	Pb^{2+}
Pb 0	136.3/141.2	Pb^{0}
I 3d	618.9/630.4	I^{-}
Br 3d	68.1/69.2	Br^{-}
CDs-PSK (Fresh)		
C 1s	284.5/285.5/287.9	C=C, C=O/ C=N
Pb 4f	138.0/142.80	Pb^{2+}
I 3d	618.80/630.30	I^{-}
Br 3d	68.0/69.0	Br^{-}
CDs-PSK (Aged)		
C 1s	284.5/285.6/288.0	C=C, C=O/ C=N
Pb 4f	138/142.8	Pb^{2+}
I 3d	618.8/630.3	I^{-}
Br 3d	68.0/69.0	Br^{-}

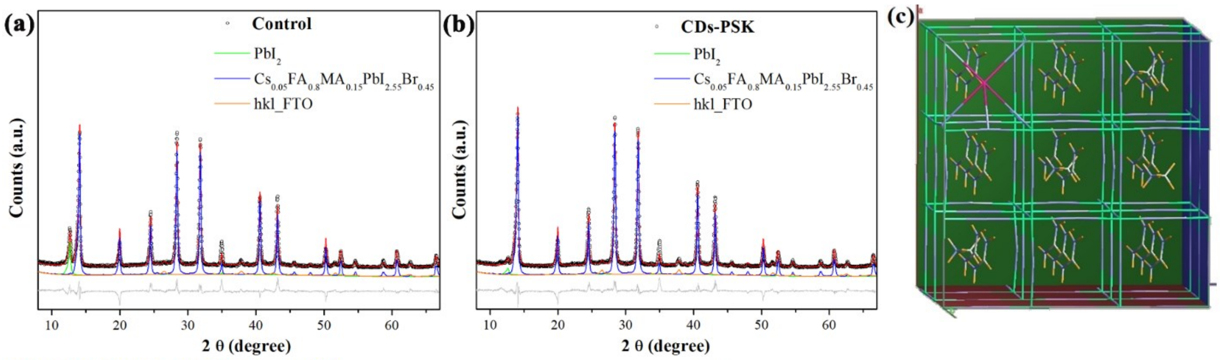

(d)

```
prm !FA_ta 0.16619  min = Val - 0.05; max = Val + 0.05;
prm !FA_tb 0.17514  min = Val - 0.05; max = Val + 0.05;
prm !FA_tc 0.09869  min = Val - 0.05; max = Val + 0.05;
prm !MA_ta =1/6; '0.12873  min = Val - 0.05; max = Val + 0.05;
prm !MA_tb =1/6; '0.20493  min = Val - 0.05; max = Val + 0.05;
prm !MA_tc =1/6; '0.16974  min = Val - 0.05; max = Val + 0.05;
macro FA(na, nb, nc)
{
rigid
  z_matrix N1##_##na##nb##nc
  z_matrix C1##_##na##nb##nc N1##_##na##nb##nc 1.2855
  z_matrix H1##_##na##nb##nc N1##_##na##nb##nc 1.0154  C1##_##na##nb##nc 124.703
  z_matrix H2##_##na##nb##nc N1##_##na##nb##nc 0.9993  C1##_##na##nb##nc 116.424 H1##_##na##nb##nc -177.231
  z_matrix H3##_##na##nb##nc C1##_##na##nb##nc 1.0865  N1##_##na##nb##nc 117.511 H2##_##na##nb##nc 1.470
  z_matrix N2##_##na##nb##nc C1##_##na##nb##nc 1.2809  H3##_##na##nb##nc 117.692 N1##_##na##nb##nc -179.927
  z_matrix H4##_##na##nb##nc N2##_##na##nb##nc 1.0152  C1##_##na##nb##nc 124.430 N1##_##na##nb##nc 0.331
  z_matrix H5##_##na##nb##nc N2##_##na##nb##nc 0.9996  C1##_##na##nb##nc 117.495 H4##_##na##nb##nc 179.631
  Translate_point_amount(N2##_##na##nb##nc, -1/2)
  rotate FA_ra -90.27387    qa 1        ' min = Val -10; max = Val +10;
  rotate FA_rb  0.66420     qb 1        ' min = Val -10; max = Val +10;
  rotate FA_rc  62.28333    qc 1        ' min = Val -10; max = Val +10;
  Translate_point_amount(N2##_##na##nb##nc, +1/2)
  translate ta = FA_ta + (na-1)/3;  tb = FA_tb + (nb-1)/3; tc = FA_tc  + (nc-1)/3;
}
macro MA(na, nb, nc)
{
rigid
  z_matrix C1##_##na##nb##nc
  z_matrix H1##_##na##nb##nc C1##_##na##nb##nc 1.0710
  z_matrix H2##_##na##nb##nc C1##_##na##nb##nc 1.0772  H1##_##na##nb##nc 111.581
  z_matrix H3##_##na##nb##nc C1##_##na##nb##nc 1.0877  H1##_##na##nb##nc 110.148 H2##_##na##nb##nc 122.742
  z_matrix N1##_##na##nb##nc C1##_##na##nb##nc 1.4632  H1##_##na##nb##nc 107.975 H2##_##na##nb##nc -118.931
  z_matrix H4##_##na##nb##nc N1##_##na##nb##nc 1.0260  C1##_##na##nb##nc 113.700 H2##_##na##nb##nc -60.390
  z_matrix H5##_##na##nb##nc N1##_##na##nb##nc 1.0114  C1##_##na##nb##nc 109.049 H4##_##na##nb##nc 119.860
  z_matrix H6##_##na##nb##nc N1##_##na##nb##nc 1.0192  H4##_##na##nb##nc 107.294 H5##_##na##nb##nc -114.270
  Translate_point_amount(N1##_##na##nb##nc, - 1/2)
  rotate MA_ra  153.22990      qa 1    ' min = Val -10; max = Val +10;
  rotate MA_rb  69.22969       qb 1    ' min = Val -10; max = Val +10;
  rotate MA_rc  132.73653      qc 1    ' min = Val -10; max = Val +10;
  Translate_point_amount(N1##_##na##nb##nc, + 1/2)
  translate ta = MA_ta + (na-1)/3;  tb = MA_tb + (nb-1)/3; tc = MA_tc + (nc-1)/3;
}
```

Figure S12. XRD patterns and corresponding rigid body assisted Rietveld refinement fittings of as-prepared perovskite films. (**a**) Control; (**b**) CDs-PSK film; (**c**) The crystal structure $Cs_{0.05}FA_{0.8}MA_{0.15}PbI_{2.55}Br_{0.45}$ with 4 MA molecules and 22 FA molecules defined as rigid body allowing their orientation to be refined in their corresponding sub-cell; (**d**) Realizing of this function in DIFFRAC.TOPAS v6 syntax

Table S2. Fitted results of the XRD patterns demonstrated in **Figure S11**. Phase composition and lattice constant of $Cs_{0.05}FA_{0.8}MA_{0.15}PbI_{2.55}Br_{0.45}$ perovskite.

Sample	$Cs_{0.05}FA_{0.8}MA_{0.15}PbI_{2.55}Br_{0.45}$					
	Lattice parameters			Crystallite size (nm) of Perovskite	Phase ratios (wt%)	
	a (Å)	b (Å)	c (Å)		Perovskite	PbI_2
Control	18.882 ±0.022	18.823 ±0.002	18.884 ±0.022	47.16 ±0.84	98.53 ±0.16	**1.47 ±0.16**
CDs-PSK	18.882 ±0.018	18.827 ±0.002	18.878 ±0.018	43.07 ±0.70	99.55 ±0.13	**0.45 ±0.13**

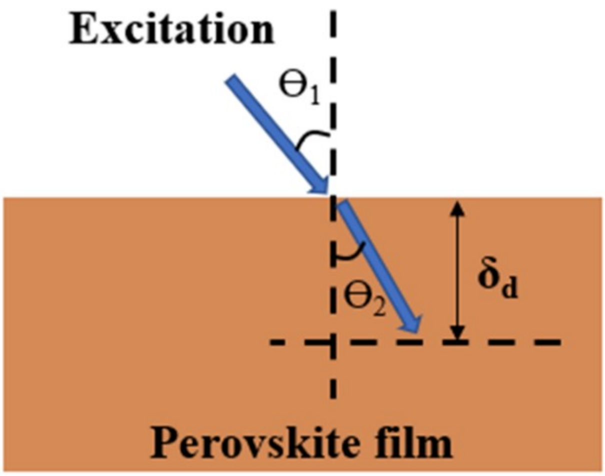

Figure S13. Schematic of incident-angle dependent PL

Estimation of penetration depth: In this work, PL was taken at very small incident angle (Θ_1 = ~0-1 °, nearly vertical to the film surface). The refraction effect was taken into consideration in this estimation process by using Snell's law $\sin\Theta_1/\sin\Theta_2 = n_2/n_1$, where n_1, n_2 are reflective index of air (~1) and perovskite film (~1.7), respectively. The absorption coefficient (α_2) of perovskite thin film at the wavelength of 405 nm is ~ 2 x 10^5 cm^{-1}.[1] Therefore, the penetration depth (δ_d) of the excitation laser (405 nm) in perovskite film is estimated by using the equation, $\delta_d = \cos\Theta_2/\alpha_2$ = ~50 nm.

Table S3. Carrier lifetime of control and CDs-PSK film deposited on glass substrate.

Sample	A_1	τ_1 (ns)	A_2	τ_2 (ns)	τ_{ave} (ns)

Control	0.87	23.89	0.21	327.16	333.50
CDs-PSK	0.87	19.02	0.20	547.44	549.44

(Where $\tau_{ave} = (A_1 \times \tau_1^2 + A_2 \times \tau_2^2)/(A_1 \times \tau_1 + A_2 \times \tau_2)$)

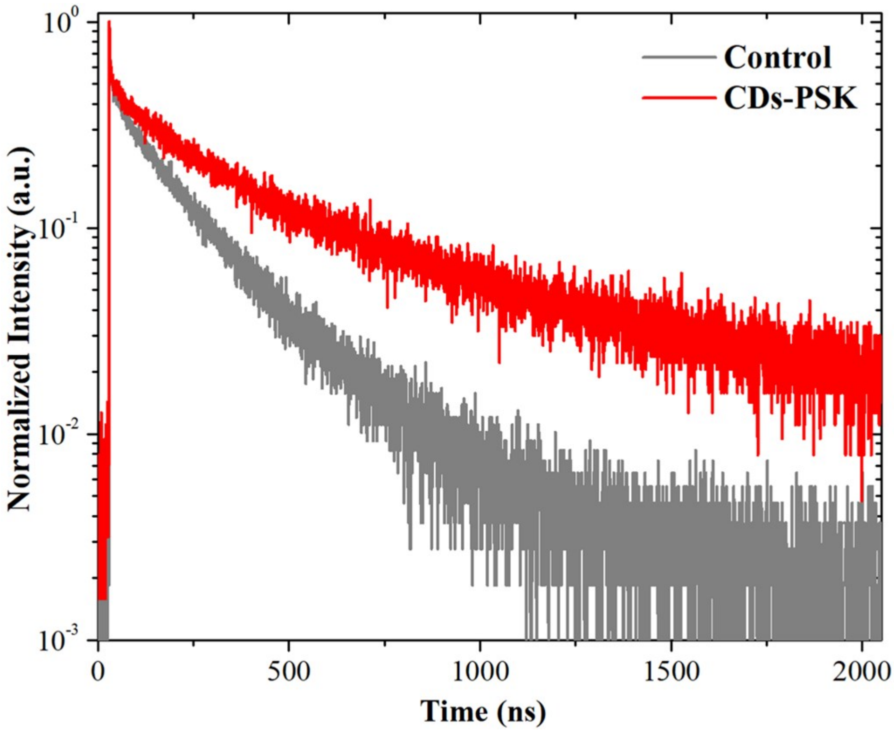

Figure S14. Time-resolved photoluminescence for perovskite films in which the incident light was from the back (glass side).

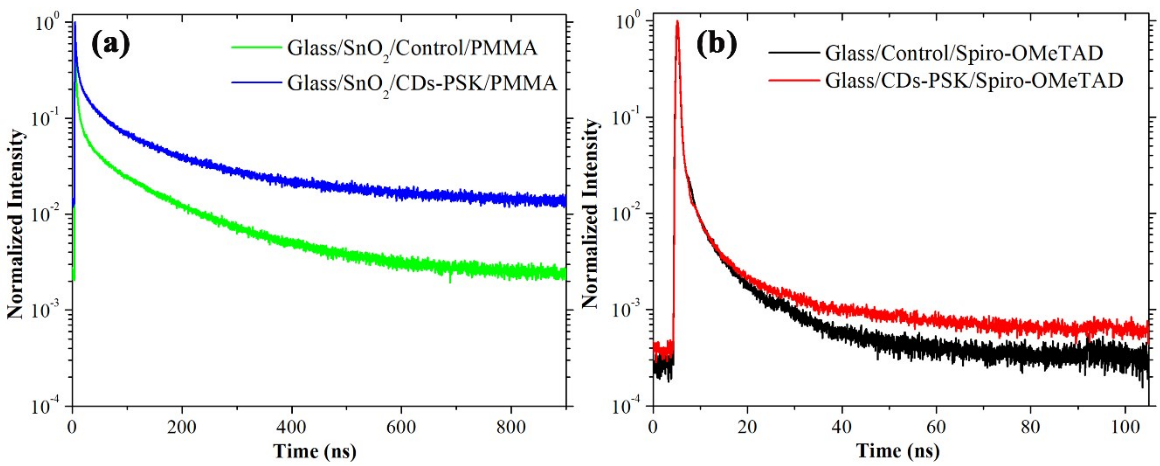

Figure S15. Time-resolved photoluminescence for perovskite films in contact with charge-separating layer. (**a**) SnO_2 (incident light direction was from glass side), (**b**) Spiro-OMeTAD (incident light direction was from PMMA side).

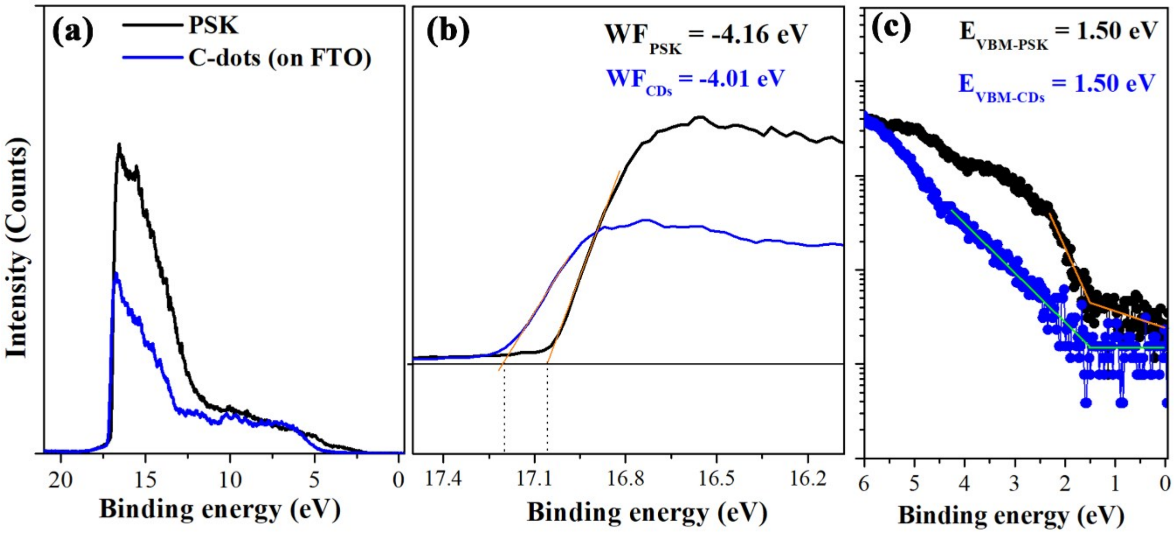

Figure S16. UPS spectra (He-Iα = 21.22 eV) of perovskite film and CDs films.

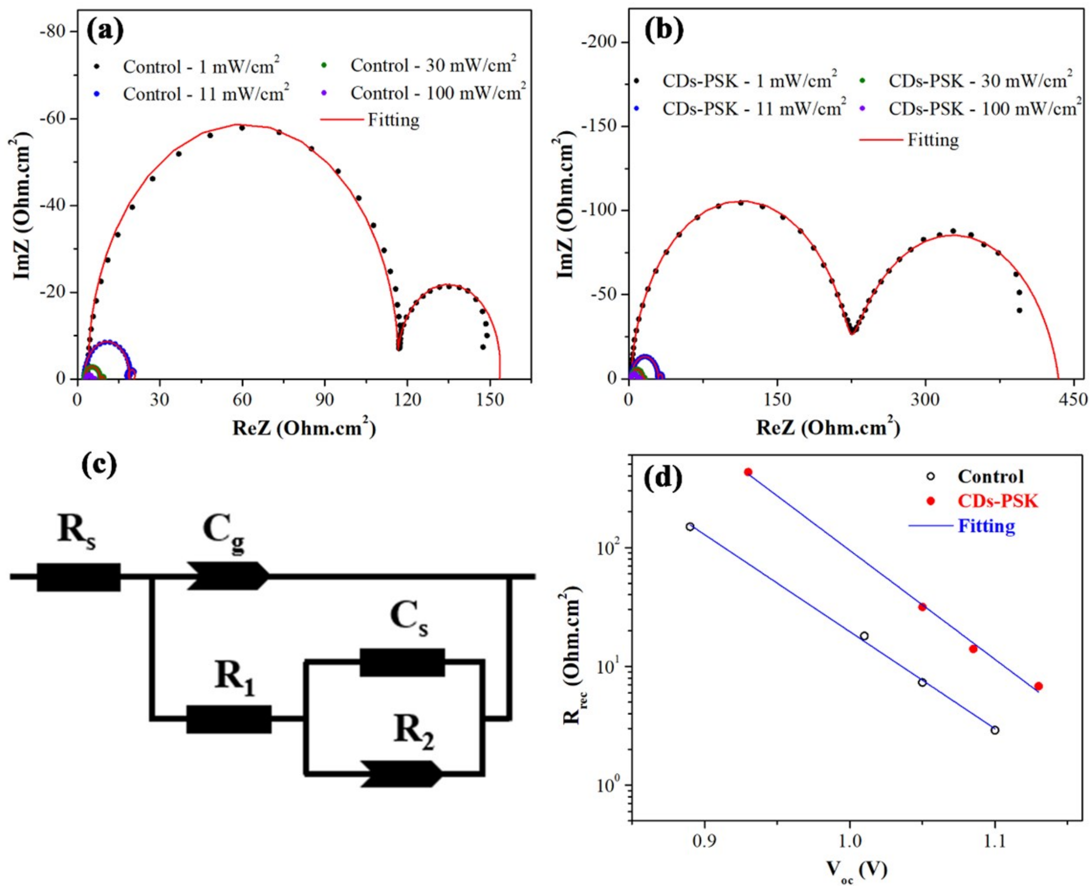

Figure S17. Nyquist plots of PSCs made using control perovskite (**a**) and CDs-PSK (**b**) measured under various light illumination intensities at open-circuit condition. Equivalent circuit used to fit the impedance spectra (**c**). Extracted recombination resistance versus open-circuit voltage (**d**). Ideality factors extracted from fitting of recombination resistance are 2.05 and 1.83 for control and CDs-PSK based PSCs, respectively.

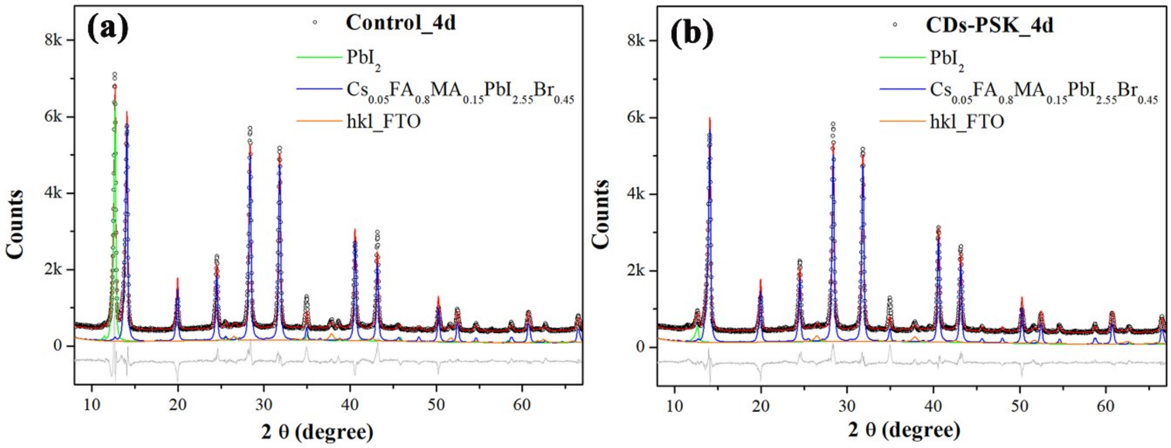

Figure S18. XRD patterns and corresponding Rietveld refinement fittings of aged perovskite films. (**a**) Control and (**b**) CDs-PSK films.

Table S4. Fitted results of the XRD patterns demonstrated in **Figure S17**. Phase composition and lattice constant of $Cs_{0.05}FA_{0.8}MA_{0.15}PbI_{2.55}Br_{0.45}$ perovskite.

Sample	$Cs_{0.05}FA_{0.8}MA_{0.15}PbI_{2.55}Br_{0.45}$					
	Lattice parameters			Crystallite size (nm) of Perovskite	Phase ratios (wt%)	
	a (Å)	b (Å)	c (Å)		Perovskite	PbI_2
Control_4d	18.874 ±0.008	18.829 ±0.003	18.888 ±0.007	41.46 ±0.76	96.89 ±0.11	**3.11 ±0.11**
CDs-PSK_4d	18.876 ±0.007	18.832 ±0.002	18.888 ±0.006	43.19 ±0.71	99.43 ±0.15	**0.57 ±015**

References

(1) De Wolf, S.; Holovsky, J.; Moon, S.-J.; Löper, P.; Niesen, B.; Ledinsky, M.; Haug, F.-J.; Yum, J.-H.; Ballif, C. Organometallic Halide Perovskites: Sharp Optical Absorption Edge and Its Relation to Photovoltaic Performance. *The Journal of Physical Chemistry Letters*. **2014**, *5*, 1035-1039.